Catalysis Today 176 (2011) 258–262

Contents lists available at ScienceDirect

Catalysis Today

journal homepage: www.elsevier.com/locate/cattod

Properties and activities of ZSM-5 + Al_2O_3 supported RuNi catalysts in 1-methylnaphthalene hydrogenation: Effect of Ru precursors

Aleksandra Masalska*

Wrocław University of Technology, Faculty of Chemistry, 7/9 Gdańska Str., 50-344 Wrocław, Poland

ARTICLE INFO

Article history:
Received 29 September 2010
Received in revised form 5 December 2010
Accepted 7 December 2010
Available online 12 January 2011

Keywords:
RuNi catalyst
Ru precursor
1-Methylnaphthalene hydrogenation

ABSTRACT

RuNi (8 wt.% NiO; 1.1 wt.% RuO_2) catalysts on ZSM-5 + Al_2O_3 were tested in the hydrogenation of 1-methylnaphthalene, and the effect of the Ru precursor on their physicochemical and catalytic properties was examined. The catalysts were analyzed by XRF, N_2-sorption, TPR, H_2-chemisorption, TPD-NH_3, XRD, XPS, TOF-SIMS, SEM and TEM. The order of their activity and stability: $[Ru(NH_3)_6]Cl_3 \sim (NH_4)_2[RuCl_6] < Ru(C_5H_7O_2)_3 < Ru_3(CO)_{12}$ correlates with the reducibility, metal dispersion, and atomic ratio of Ni/Al + Si on the catalyst surface.

1. Introduction

The use of components from destruction processes for diesel oil production leads to an increase in aromatic content (*e.g.* FCC [1]), as well as to the deterioration of cold flow properties (*e.g.* hydrocracking [2]). High aromatic content affects fuel quality (by lowering the cetane number and combustion characteristics) and contributes notably to the formation of toxic emissions (NO_x, particulate matter). If the standard demands placed on diesel oil are to be met, the use of dewaxing and aromatic hydrogenation processes becomes necessary. Our recent study shows that dewaxing catalysts (NiO (8 wt.%)/ZSM-5 + Al_2O_3) with hydrogenating functions enhanced by Ru incorporation (0.9 wt.% RuO_2) enable simultaneous conversion of n-alkanes and arenes [3], and that the effect of Ru (1.1 wt.% RuO_2) depends on the Ni incorporation and calcination procedures used [4]. Many researchers have reported that the nature of the Ru precursor largely influences the physicochemical properties and activities of the catalysts [5–9]. Most consideration has been given to the contribution of such precursors as $RuNO(NO_3)_3$ [5,6,8], $RuCl_3$ [6–8], $[Ru(NH_3)_6]Cl_3$ [7,9], $Ru(C_5H_7O_2)_3$ [5–7] and $Ru_3(CO)_{12}$ [5,6]. The results that have been published so far pertain primarily to monometallic 0.5–5 wt.% Ru catalysts on supports containing alumina [6], silica, mesoporous materials [9], carbon [8] or zeolites (Y, β [7], KL [5]). The activities of those catalysts were tested in the reactions of hydrogenolysis [6,7], selective hydrogenation [5] or NH_3 synthesis [8]. The problem of how the nature of the Ru precursors affects the hydrogenating activity of dewaxing catalysts has been left without due consideration in the literature. Therefore, it seemed advisable to examine the effect of Ru precursors on the physicochemical properties of RuNi/ZSM-5 + Al_2O_3 catalysts (1.1 wt.% RuO_2, 8 wt.% NiO) and their hydrogenating function, which is expressed in terms of their activity in 1-methylnaphthalene (1-MN) hydrogenation.

2. Experimental

2.1. Catalyst preparation

RuNi (8 wt.% NiO; 1.1 wt.% RuO_2) catalysts were obtained by the impregnation of the Ni catalyst with ruthenium(III) acetylacetonate (RuNi/A), triruthenium dodecacarbonyl (RuNi/B), hexaammineruthenium(III) chloride (RuNi/C) or ammonium hexachlororuthenate (RuNi/D). After the drying stage (50 °C, 0.04 MPa, 3 h), the precursors were decomposed in H_2 flow (500 °C, 0.1 MPa, 3 h). To prevent Ru particle agglomeration, which occurs at about 150 °C in air [10], the catalysts were also cooled in H_2 flow. The Ni/ZSM-5 + Al_2O_3 (1:1) catalyst was prepared by mixing Ni,H-ZSM-5 zeolite (SiO_2/Al_2O_3 molar ratio of 35:1) and aluminium hydroxide powders. Ni precursor ($Ni(NO_3)_2$) was incorporated in a two-step procedure: one half (4 wt.% of NiO) during the support formation (F), and the other half by impregnation (I). After stages F and I, the catalyst was dried and calcined in air (400 °C, 2 h).

2.2. Catalyst characterization

Porous structure and acidity. N_2 adsorption was measured at 77 K (Quantachrome, AUTOSORB-1). Acidity was determined by the NH_3-TPD method [4].

* Tel.: +48 71 320 63 02; fax: +48 71 322 15 80.
E-mail address: Aleksandra.Masalska@pwr.wroc.pl

0920-5861/$ – see front matter © 2010 Elsevier B.V. All rights reserved.
doi:10.1016/j.cattod.2010.12.018

Table 1
Effect of Ru precursor on physicochemical properties.

Catalyst code	Ru precursor	NiO[a] (wt.%)	RuO_2[a] (wt.%)	S_{BET} (m^2/g)	Pore volume (cm^3/g)		APD[b] (nm)	V_{H_2}[c] (cm^3/g)	H_2 uptake[d] (a.u.)	a_{NH_3}[e] (mmol/g)
					V_T	V_{MIK}				
RuNi/A	$Ru(C_5H_7O_2)_3$	8.0	1.09	253	0.32	0.041	5.6	1.72	866	0.89
RuNi/B	$Ru_3(CO)_{12}$	8.1	1.08	260	0.33	0.042	5.4	2.17	1055	0.88
RuNi/C	$[Ru(NH_3)_6]Cl_3$	8.0	1.12	250	0.32	0.038	5.3	1.48	685	0.97
RuNi/D	$(NH_4)_2[RuCl_6]$	7.9	1.13	257	0.34	0.034	5.2	1.47	701	1.08

[a] By XRF.
[b] Average pore diameter (BHJ method).
[c] Volume of H_2 adsorbed.
[d] Reducibility up to 500 °C (TPR).
[e] Acidity by NH_3-TPD.

XRD examinations. XRD patterns were obtained using a PANalytical X'Pert ProMPD diffractometer (Holland) with a PW3050/65 goniometer, at 40 kV and 30 mA (CuKα).

Chemical analysis. Ni and Ru content was determined by XRF (Canberra Packard, 1510), and surface composition by TOF-SIMS (ION-TOF, TOF-SIMS IV) and XPS (SPECS, UHV/XPS PHOIBOS 100).

H_2 chemisorption and TPR. The H_2 volume adsorbed was measured after reduction in H_2 (500 °C, 1 h) (Micromeritics, ASAP 2010C). TPR was carried out up to 850 °C (Polska, Peak-5) [4].

Surface morphology. SEM was performed using a JSM5800LV microscope (JEOL) with ISIS300 system for microanalysis (Oxford). HRTEM images and selected area electron diffraction (SAED)

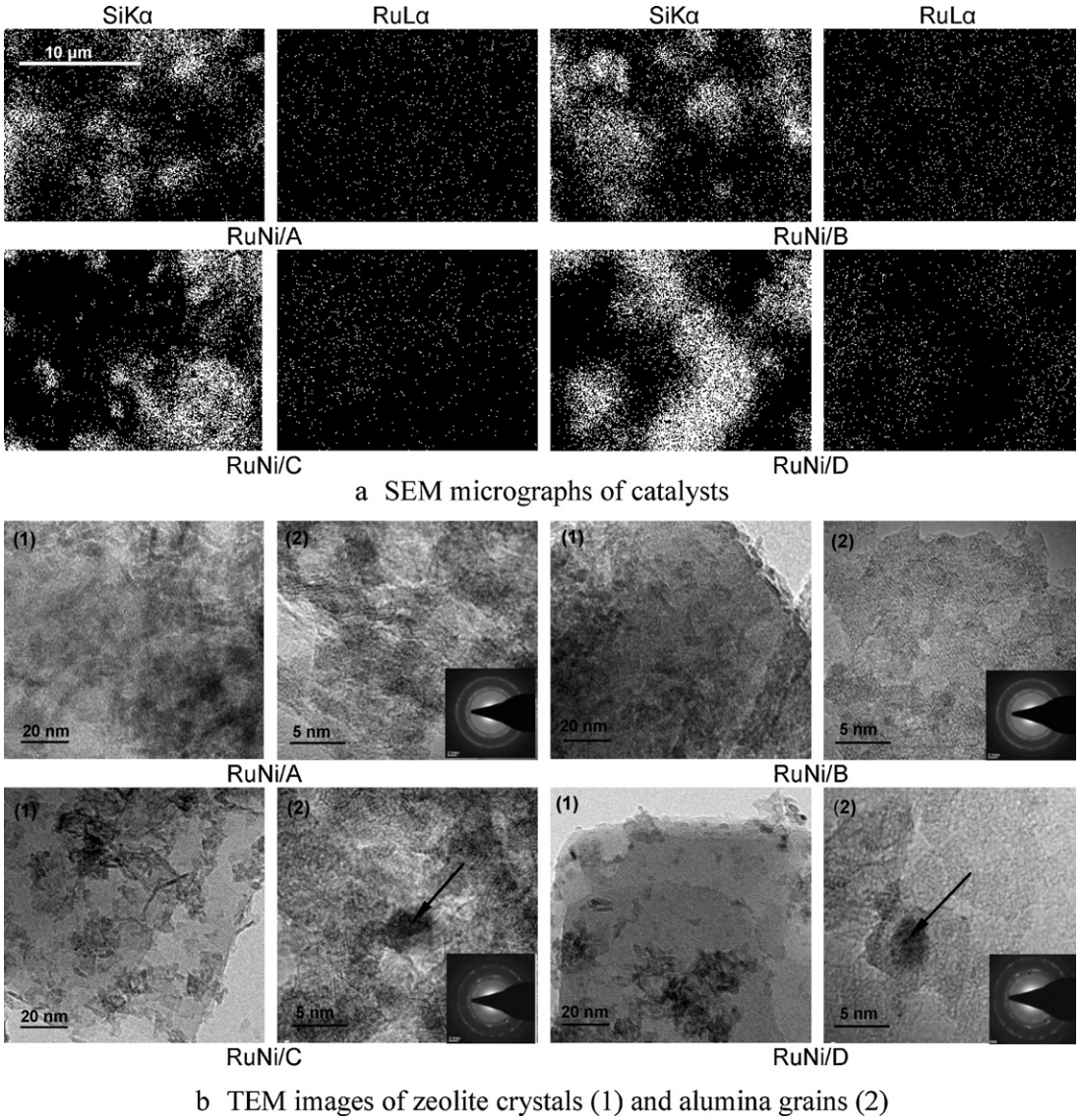

Fig. 1. Effect of Ru precursor on RuNi catalyst surface morphology: (a) distribution of Si and Ru (SEM micrographs) and (b) zeolite crystals (1) and alumina grains (2) (TEM images).

patterns were obtained with a Philips CM-20 SuperTwin microscope.

Catalytic experiments. Catalyst activity was tested in 1-methylnaphthalene (1-MN) hydrogenation in a fixed-bed reactor at atmospheric pressure. The catalyst (100 mg) was activated in H_2 flow for 1 h up to 500 °C, the heating rate being 5°/min. Products were analyzed on-line by gas chromatography [4].

3. Results and discussion

The physicochemical properties of the catalysts are compiled in Table 1. Regardless of the Ru precursor applied, the textures of the RuNi catalysts were similar. None of the catalysts examined displayed XRD lines typical of Ni and Ru and their compounds (not shown), which is attributable to the high dispersion or the poor crystallinity of these species.

SEM observations have disclosed the uniformity of Ni distribution across the surface of all catalysts (not shown), but Ru distribution across RuNi/A and RuNi/B (Ru precursors soluble in organic solvents) is more uniform than across RuNi/C and RuNi/D (Ru precursors soluble in water) (Fig. 1a). With precursors soluble in water, Ru distribution on the catalyst surface prepared with $(NH_4)_2[RuCl_6]$ was more irregular as compared to $[Ru(NH_3)_6]Cl_3$, owing to the pH of the impregnating solutions (6 and 10, respectively). At a pH of the solution lower than their PZC (point of zero charge), solid surfaces adsorb anions, at a pH higher than their PZC, they adsorb cations [11]. Since the PZC of alumina and zeolite were 7–9 and 4, respectively, $[Ru(NH_3)_6]^{3+}$ cations adsorbed both on alumina and zeolite, whereas $[RuCl_6]^{2-}$ anions adsorbed preferentially on alumina.

All HRTEM images disclose large zeolite crystals covered with alumina grains (not shown). Characteristic images of zeolite crystals and alumina grains are visualized in Fig. 1b. Neither SAED patterns nor HRTEM images of the zeolite crystal surface reveal reflections or lattice fringes typical of Ni (2.03; 1.76; 1.24 and 1.05 Å) or Ru (2.34; 2.14; 2.06; 1.58; 1.35 and 1.22 Å). No Ni or Ru particles are present on the alumina grains of the catalysts prepared with $Ru(C_5H_7O_2)_3$ and $Ru_3(CO)_{12}$, which suggests high metal dispersion. Relevant SAED patterns show only rings typical of γ-Al_2O_3 (2.37; 1.97 and 1.39 Å). Although most alumina grain images for the catalysts prepared with Ru precursors soluble in water fail to reveal metal particles, some alumina grains are densely covered with metal particles (Fig. 1b; 3–5 nm metal particles with 0.2 nm lattice fringes). Since the distances between Ni and Ru lattice planes are similar (Ni (1 1 1)–2.03 Å, Ru (1 0 1)–2.06 Å), it is difficult to identify the metal type only by HRTEM.

It is difficult to compare our observations of the effect of Ru precursors on metal distribution and dispersion with the observations made by other authors. The catalysts chosen for their studies differ noticeably in chemical composition, preparation method and the nature of the Ru precursors. Álvarez-Rodríguez et al. [5] found that Ru particles on the Ru(2%)/KL catalyst were smaller with $Ru_3(CO)_{12}$ (2.8 nm) than $Ru(C_5H_7O_2)_3$ (7.3 nm). Maroto-Valiente et al. reported similar results for Ru(1%)/Al_2O_3 catalysts [6]. Testing Ru(5%) catalysts on β and Y, Preda et al. [7] found that the mean size of Ru particles on the catalyst prepared with $[Ru(NH_3)_6Cl_3]$ was smaller (23.1 nm on β and 36.1 nm on Y) compared to the one prepared with $Ru(C_5H_7O_2)_3$ (63.7 nm on β and 74.3 nm on Y), which is inconsistent with our findings.

All TPR profiles (Fig. 2) display high-temperature reduction regions with a maximum at 780 °C (ascribed to the reduction in Ni–Al oxide spinels due to the strong interactions between Ni oxide species and alumina [12]); they also show strongly differentiated reduction regions up to 220 °C, 220–450 °C and 450–600 °C. H_2 uptake at 450–600 °C suggests a reduction in the amorphous over-

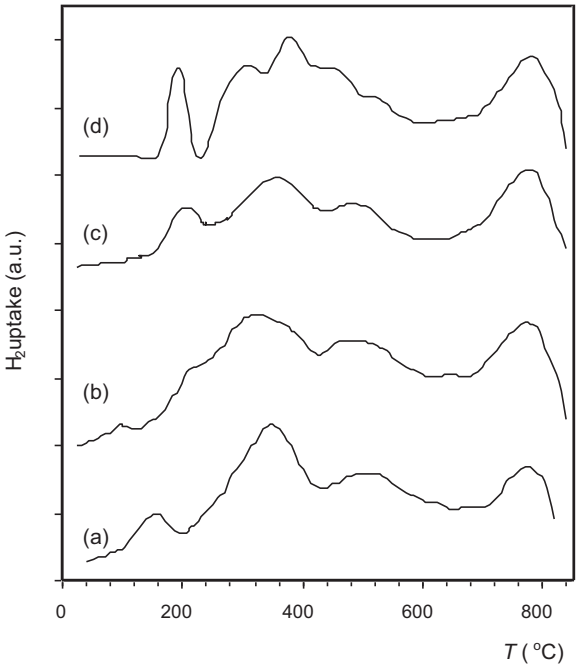

Fig. 2. TPR profiles of catalysts: (a) RuNi/A, (b) RuNi/B, (c) RuNi/C, and (d) RuNi/D.

layer of NiO, which is not chemically bound but interacts with the support more strongly than does NiO, which reduces below 450 °C. Up to 220 °C the highest H_2 uptake is observed over RuNi/D. The presence of a separate signal implies that RuO_2 tends to occur as a separate phase, but interacts with the support or NiO ("pure" RuO_2 undergoes reduction at 120–150 °C [12]). The presence of low-temperature reduction regions on the RuNi/A and RuNi/C profiles implies that a certain amount of Ru occurs in the form of bimetallic NiRu oxide clusters. The RuNi/B profile shows no peak typical of RuO_2 reduction; apparently, only such clusters are present in this catalyst (the strongest interaction being Ru–Ni).

The effect of the nature of the Ru precursor on the composition of the RuNi catalyst surface was measured by XPS and TOF-SIMS (Table 2). XPS results (upon deconvolution of the Ni $2p_{3/2}$ region) show that the highest reducibility (with Ni^0 proportion of 24%) was that of RuNi/B. Most of the Ni–Al oxide spinels occurred on RuNi/C and RuNi/D surfaces. The nature of Ru precursors notably affects the concentration of Ni atoms on the catalyst surface. The atomic Ni/Al + Si and Ni/Ru ratios for RuNi/B are the highest. TOF-SIMS analyses show similar positive secondary ion mass spectra for all catalysts; of the Ni and Ru containing ions, Ni^+ (small amounts of NiO^+, $NiOH^+$ and traces of $NiOH_2^+$) and Ru^+ (no signals from other Ru containing ions) dominate on the catalyst surface. Negative secondary ion mass spectra display the presence of Cl^- on the surfaces of RuNi/C and RuNi/D, which suggests incomplete decomposition of Ru precursor and/or incomplete Cl^- removal from the catalyst surface. With a larger amount of Cl^- on its surface, RuNi/D shows a higher acidity (NH_3-TPD) (Table 1). Acidity was also reported to increase upon chlorine addition [13]. Apart from Cl^-, no secondary anions including Cl or Ru are detected. TOF-SIMS corroborates the high reducibility of RuNi/A and RuNi/B detected by TPR. The NiO^+/Ni^+ and $NiOH^+/Ni^+$ intensity ratios are much lower for these catalysts than for RuNi/C and RuNi/D (Table 2). TOF-SIMS confirms the highest concentration of Ni atoms on the RuNi/B surface (detected by XPS). The Ni^+/Ru^+ intensity ratio for RuNi/B is three times that for RuNi/D.

The hydrogenation actitivity of RuNi/ZSM-5 + Al_2O_3 was tested at 200–260 °C; this was the range over which the catalysts displayed dewaxing properties [3]. Activity tests have shown

Table 2
Characteristics of catalyst surface.

Catalyst code	TOF-SIMS method (H_2, 500 °C, 3 h)				XPS method (H_2, 500 °C, 1 h)				
	Cl^-/total[a]	Intensity ratios of selected ions			Atomic ratio		Amount of Ni (at. %)		
		Ni^+/Ru^+	NiO^+/Ni^+	$NiOH^+/Ni^+$	Ni/Ru	Ni/Al + Si	Ni^0[b]	NiO[c]	$NiAlO_4$[d]
RuNi/A	0.2×10^{-2}	23.2	1.8×10^{-3}	2.3×10^{-2}	8	0.062	21	66	13
RuNi/B	0.2×10^{-2}	24.8	1.7×10^{-3}	1.8×10^{-2}	9	0.069	24	62	14
RuNi/C	1.3×10^{-2}	7.6	3.0×10^{-3}	3.3×10^{-2}	7	0.060	17	61	22
RuNi/D	2.4×10^{-2}	7.5	2.9×10^{-3}	3.3×10^{-2}	7	0.057	17	65	18

[a] Ratio of Cl^- ion counts to total ion counts.
[b] BE = 853.1 eV.
[c] BE = 855.6 eV.
[d] BE = 857.2 eV.

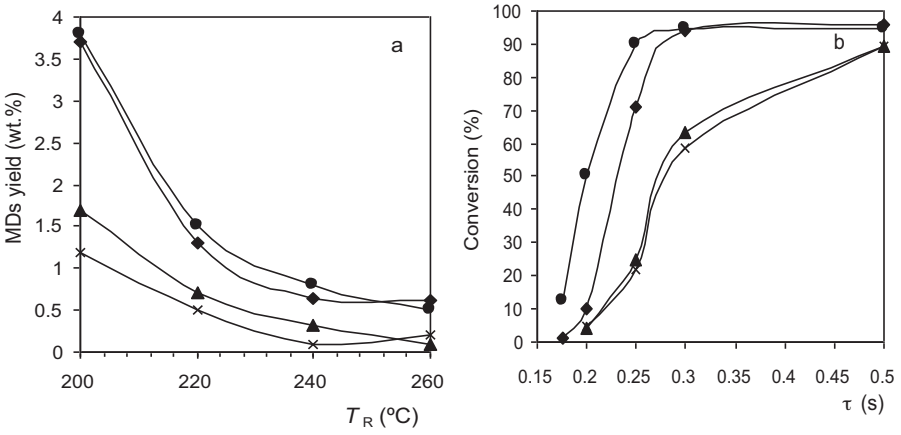

Fig. 3. Effect of reaction temperature on MD yield (τ = 0.5 s) (a) and effect of contact time on 1-MN conversion (200 °C) (b). Catalyst: RuNi/A (♦), RuNi/B (●), RuNi/C (▲), and RuNi/(D (×).

that 1-MN conversion over RuNi/B and RuNi/A (prepared with $Ru_3(CO)_{12}$ and $Ru(C_5H_7O_2)_3$) is by 4–8% and by 2–5% higher, respectively, than over RuNi/C and RuNi/D (prepared with $[Ru(NH_3)_6]Cl_3$ and $(NH_4)_2[RuCl_6]$)) (Table 3). Mainly methyltetralins (MTs) and small amounts of methyldecalins (MDs) were detected in the reaction products. Over RuNi/A and RuNi/B, the MD yield was slightly higher (Fig. 3a). Under the testing conditions applied (atmospheric pressure), this is an indication of better hydrogenating properties. The same catalysts displayed a higher stability (1-MN conversion did not decrease after the cycle of temperature effect examinations, Table 3). Their increased activity and stability were confirmed by activity tests with various contact times (Table 3, Fig. 3b). However, RuNi/B (obtained with $Ru_3(CO)_{12}$) shows slightly better catalytic properties than RuNi/A (prepared with $Ru(C_5H_7O_2)_3$). According to 1-MN conversion at contact time lower than 0.3 s (Fig. 3b), the activities of the catalysts can be ordered as: RuNi/B > RuNi/A > RuNi/C ~ RuNi/D. Catalysts with better hydrogenating properties exhibit higher NiO reducibility (TPR, XPS, TOF-SIMS), better metal dispersion (H_2 chemisorption) and more uniform Ru distribution (SEM, TEM).

Table 3
Effect of Ru precursors on RuNi catalyst activity for 1-MN conversion (τ = 0.5 s).

Catalyst code	Reaction temperature (°C)					
	200	220	240	260	200[a]	200[b]
	Conversion (%)					
RuNi/A	95.7	81.4	57.8	36.4	95.8	22.1
RuNi/B	96.6	86.1	63.0	38.2	95.8	22.3
RuNi/C	92.3	77.9	56.2	31.9	89.2	3.3
RuNi/D	92.5	78.8	55.3	31.3	89.4	8.0

[a] After activity test cycle including the effect of reaction temperature.
[b] After the whole activity test including the effect of both temperature and contact time.

4. Conclusions

Among the Ru precursors ($Ru(C_5H_7O_2)_3$, $Ru_3(CO)_{12}$, $[Ru(NH_3)_6]Cl_3$, $(NH_4)_2[RuCl_6]$) used in this study, $Ru_3(CO)_{12}$ made it possible to prepare a RuNi catalyst with the strongest Ru–Ni interactions, the highest metal oxide reducibility, enhanced metal dispersion, a uniform Ru distribution, and a high concentration of Ni atoms on its surface. These are the properties that upgraded the hydrogenation function of this dewaxing catalyst.

Acknowledgements

The author thanks the Ministry of Science and Higher Education for financial support (N205 066 31/3012) and Prof. Leszek Kępiński (Institute of Low Temperature and Structure Research, Polish Academy of Sciences, Wroclaw) for performing TEM analysis.

References

[1] B.H. Cooper, B.B.L. Donnis, Appl. Catal. A: Gen. 137 (1996) 203.
[2] I. Skręt, Bulletin of Institute of Petroleum Processing, 2000, p. 296 (ISSN, 1233-3867 XII/4).
[3] A. Masalska, Catal. Today 137 (2008) 439.
[4] A. Masalska, Catal. Lett. 127 (2009) 158.

[5] J. Álvarez-Rodríguez, A. Guerrero-Ruiz, et al., Catal. Today 107–108 (2005) 302.
[6] A. Maroto-Valiente, M. Cerro-Alarcón, et al., Appl. Catal. A: Gen. 283 (2005) 23.
[7] R. Preda, V.I. Pârvulescu, A. Petride, A. Banciu, et al., J. Mol. Catal. A: Chem. 178 (2002) 79.
[8] I. Rossetti, L. Forni, Appl. Catal. A: Gen. 282 (2005) 315.
[9] M. Hartmann, C. Bishof, Z. Luan, L. Kevan, Micropor. Mesopor. Mater. 44–45 (2001) 385.
[10] P. Tian, J. Blanchard, K. Fajerwerg, M. Breysse, et al., Micropor. Mesopor. Mater. 60 (2003) 197.
[11] M. Schreier, J.R. Regalbuto, J. Catal. 225 (2004) 190.
[12] J.M. Rynkowski, T. Paryjczak, M. Lennik, Appl. Catal. A: Gen. 126 (1995) 257.
[13] A.K. Aboul-Gheit, A.E. Awadallah, N.A.K. Aboul-Gheit, E.S.A. Solyman, M.A. Abdel-Aaty, Appl. Catal. A: Gen. 334 (2008) 304.